A Method for Calibrating Diffusion Gradients in Diffusion Tensor Imaging

Yu-Chien Wu, MD, PhD,†§ and Andrew L. Alexander, PhD†‡§*

Objective: To calibrate and correct the gradient errors including gradient amplitude scaling errors, background/imaging gradients, and residual gradients in diffusion tensor imaging (DTI).

Methods: A calibration protocol using an isotropic phantom was proposed. Gradient errors were estimated by using linear regression analyses on quadratic functions of diffusion gradients along 3 orthogonal directions. A 6-element total effective scaling vector is generated from the calibration protocol to retrospectively correct gradient errors in DTI experiments.

Results: The accuracy of the calibration protocol was within 1% or less in estimating gradient scaling errors. On both the brain study and the computer simulations, the retrospective correction minimized undesirable estimate biases of DTI measurements due to gradient errors.

Conclusion: The protocol and retrospective correction are shown to be effective. The method may be used for prospective correction if actual diffusion-gradient waveforms are available. The methodology is expandable to general diffusion imaging schemes.

Key Words: gradient calibration, background gradient, residual gradient, imaging gradient, diffusion tensor imaging

(*J Comput Assist Tomogr* 2007;31:984–993)

Diffusion tensor imaging (DTI) is a noninvasive magnetic resonance imaging method for measuring microstructural information about biological tissues.[1,2] The clinical and research applications of DTI are rapidly expanding. The trace of the diffusion tensor (DT) describes the magnitude of diffusion in tissues. Measures of diffusion anisotropy appear to be highly sensitive to changes in tissue microstructure. Further, white matter tractography algorithms may be used to estimate patterns of white matter connectivity using the major eigenvector.

In 1965, Stejskal and Tanner proposed methods for diffusion-weighted (DW) nuclear magnetic resonance using gradient pulses.[3] Imperfections of diffusion-weighting gradients may cause errors in estimating the mean diffusivity (MD; trace divided by 3), the fractional anisotropy (FA), and the tensor orientation.[4–6] The gradient imperfections may be classified into 3 categories: (1) gradient errors with constant directions including background and imaging gradients, (2) gradient errors whose directions are associated with diffusion-weighting gradients including gradient scaling and residual gradients, and (3) spatial nonuniformity and nonlinearity.

Background gradients and imaging gradients may be the most significant sources of gradient errors.[5] Many research studies have demonstrated that using opposite diffusion-weighting gradient polarities can eliminate the cross-terms of background gradients[7–11] and imaging gradients.[12–15] Residual gradients arising from long-term Eddy currents can also be corrected by reversing diffusion-weighting gradients to estimate the symmetry of distortions through a cross-correlation approach.[16] Finally, Bammer et al[17] developed a method to estimate and correct errors relating to gradient spatial uniformity and linearity using an isotropic water phantom.

Herein, we propose a calibration method that uses these correction strategies described above and the basic concept of gradient errors to form a more comprehensive correction protocol. Similar to previous research studies, this method takes advantage of opposite diffusion-weighting gradient polarities and an isotropic phantom. However, the difference is that this method acquires images at multiple diffusion-weighting levels along 3 orthogonal directions, instead of single diffusion-weighting used in previous studies.[9–11,14–16] The gradient errors may be estimated through linear regression analyses (one on combined images of opposite gradient polarities and one on images of single polarity) on quadratic functions of the diffusion gradients. A 6-element total effective scaling vector is generated for retrospective correction. This approach corrects all possible gradient errors in a single calibration protocol and is potential for prospective gradient correction if gradient waveforms are available. This protocol does not attempt to calibrate the spatial errors of diffusion-weighting gradients, but there should be no difficulties in combining with the method developed by Bammer et al,[17] which also uses an isotropic phantom.

In this article, a calibration protocol and gradient error estimation framework are described. The calibration protocol may be applied on a regular basis (ie, weekly) to monitor gradient performances over time and compare measurements between scanners. The calibration protocol lasts less than 10

From the *Department of Radiology, †Waisman Laboratory for Brain Imaging and Behavior, and Departments of ‡Psychiatry and §Medical Physics, University of Wisconsin–Madison, Madison, WI.

Received for publication October 24, 2006; accepted February 16, 2007.

Reprints: Yu-Chien Wu, MD, PhD, Waisman Laboratory for Brain Imaging and Behavior, Waisman Center, University of Wisconsin-Madison, Room T231, 1500 Highland Ave, Madison, WI 53705-2280 (e-mail: yuchienwu@wisc.edu).

This study was supported by grants from the National Institutes of Health (grants MH062015, HD035476, MH069315, and NS050466), the Dana Foundation, and the National MS Society (Translational Research Partnership Grant).

minutes and is independent of DTI experiments. Therefore, for regular DTI experiments, it does not require any additional images for the purpose of gradient calibration. A retrospective correction is demonstrated on both brain DTI experiments and computer simulations. If the gradient errors are not expected to change dramatically from time to time, the same correction vector may be applied between calibration periods.

THEORY

Estimations of Gradient Scaling Factor, Residual Gradients, and Background Gradients

The gradient amplitude scaling factor (c) and residual gradients (G_r) change with the polarity of the diffusion gradients. They may be estimated using linear regression analysis of the geometric mean of the DW signals, S_+ and S_-, with opposite diffusion-weighting polarities. The geometric mean eliminates background and image gradient effects[7–15] and leaves the gradient scaling and residual gradient effects for calibration. The linear regression model is

$$\ln(\sqrt{S_+ \cdot S_-}/S_o) = \beta_2 G^2 + \beta_1 G + \beta_o + \varepsilon \quad (1)$$

where G is the prescribed gradient strength, S_o is the intensity without diffusion-weighting, β's are the model coefficients, and ε is the model error. The estimated diffusion coefficient from the calibration experiment, D_{cal}, is calculated as

$$D_{cal} = \frac{\beta_2}{B} \quad (2)$$

where $B(\delta,\Delta) = -(\gamma\delta)^2(\Delta - \delta/3)$. If the true diffusion coefficient (D_{true}) of the isotropic phantom is known, the signal attenuation has the form as

$$\ln(\sqrt{S_+ \cdot S_-}/S_o) = D_{true}[Bc^2G^2 + R_1 G_r c G + R_2 G_r^2] \quad (3)$$

where R_1 and R_2 are functions of time intervals related to the diffusion-weighting gradients waveforms. Note that the analytical expression of R_1 and R_2 may be derived if the gradient waveforms are available. Appendix A shows an example of deriving R_1 and R_2 for a simplified waveform. From Eqs. (1) and (3), the gradient scaling factor is estimated using the coefficient of the second-order term:

$$c = \sqrt{\beta_2/BD_{true}} = \sqrt{D_{cal}/D_{true}} \quad (4)$$

In addition, the strength of residual gradient is estimated using the coefficient of the first-order term:

$$G_r = \beta_1/(cD_{true}R_1). \quad (5)$$

To estimate the background gradient, the effects of the residual gradients and gradient scaling must be first eliminated, which is done by scaling the prescribed gradient strength to the corrected strength, $G_c = c_{effR}G$. c_{effR} is the effective scaling factor for correcting residual gradients and the gradient scaling:

$$c_{effR}^2 = c^2 + \frac{\beta_1}{BGD_{true}}. \quad (6)$$

See Appendix A for the derivation of c_{effR}. The strength of background gradients may be subsequently estimated using linear regression to another quadratic polynomial [see Appendix B, Eqs. (A.6) and (A.7)] of a single-gradient polarity. The background gradient is calculated by

$$G_o = \beta_{c1}/(D_{true}O_1) \quad (7)$$

and the effective scaling factor for correcting the background gradient is

$$c_{effO\pm}^2 = 1 \pm \frac{\beta_{c1}}{BGD_{true}}, \text{ for positive } (+) \text{ and negative } (-) \text{ polarity.} \quad (8)$$

See Appendix B for detailed discussions of G_o, β_{c1}, $c_{effO\pm}$, and O_1. Note that actual gradient waveforms are required to estimate G_r [Eq. (5)] and G_o [Eq. (7)] for prospectively correcting diffusion weighting by compensating amplitudes of diffusion gradients in future experiments. However, the retrospective correction does not require gradient waveforms and is described below.

Total Effective Scaling Vector and Retrospective Correction of DTI Data

The total effective scaling factor is defined as the multiplication of c_{effR} and $c_{effO\pm}$. By combining the total effective factors of 3 physical and corresponding antipodal directions ($\pm x$, $\pm y$, and $\pm z$), the total effective scaling vector becomes a 6-element vector:

$$\vec{c}_{eff} = [c_{eff+x}\ c_{eff-x}\ c_{eff+y}\ c_{eff-y}\ c_{eff+z}\ c_{eff-z}] \quad (9)$$

Accurate measurements of the waveforms of residual gradients, background gradients, and the associate functions (R_1 or O_1) are not required to estimate c_{effR} and c_{effO}. These factors are estimated directly using the results of regression analyses: β_1 and β_{c1} [see Eqs. (6) and (8)]. Also note that these factors decrease as the diffusion gradient strength increases because G is the denominator.

In the discussion below, the DT encoding formalism described by Hasan et al[18] is used. To best estimate the true diffusion measurement, the diffusion-encoding gradient ($\vec{g} = [g_x\ g_y\ g_z]$) must be corrected by the total effective scaling vector. Thus, the true diffusion-tensor elements, $\hat{\vec{d}}_{true}$, may be estimated by singular value decomposition of the following formula:[18]

$$\ln(S/S_o) = b\hat{\vec{d}}_{true} \cdot \vec{h}_{corr} \quad (10)$$

where the corrected diffusion-encoding vector is

$$\vec{h}_{corr} = [c_{effx}^2 g_x^2\ c_{effy}^2 g_y^2\ c_{effz}^2 g_z^2\ 2c_{effx}c_{effy}g_xg_y\ 2c_{effx}g_xg_z\ 2c_{effy}c_{effz}g_yg_z] \quad (11)$$

Note that positive components of $\vec{g}$ are scaled by c_{eff+} and negative components are scaled by c_{eff-}.

MATERIALS AND METHODS

Diffusion-Weighted Image Calibration

An isotropic liquid phantom containing n-undecane was used for DW image calibration experiments. Because the

diffusivity depends upon temperature, the phantom temperature was measured before each calibration experiment. The true diffusivity, D_{true}, was estimated by interpolating the temperature function described by Tofts et al.[19]

Calibration of DW imaging was performed on a 3.0T magnetic resonance imaging scanner (GE Signa; GE Healthcare, Waukesha, Wis) using a single-shot, spin echo, echo-planar imaging pulse sequence with diffusion encoding measurements obtained in 3 orthogonal directions (x, y, and z). For each direction, 46 images were acquired at different gradient strengths (from $-G_{max}$ to G_{max}) that corresponded to equal steps in b value between 0 and 1000 s/mm^2. Several of the measurements were repeated to increase the number of degrees of freedom for statistical analysis. Each image had a slice thickness of 3 mm, a matrix size of 100 × 100, a field of view of 18 cm, and TE/TR of 74/3000 milliseconds. The diffusion gradient timing parameters δ (duration) and Δ (separation from onset to onset) were 21 and 32 milliseconds, respectively. The maximum diffusion gradient (G_{max}) was 3.5 G/cm. The overall imaging time was roughly 7 minutes. A region of interest (ROI; 60% of the phantom) was selected at the center of the phantom image. The mean signal intensity in the ROI was measured for each image. As described in the "Theory" section, the linear regression analyses were performed to estimate gradient errors and the total effective scaling vector. The gradient scaling factor c was calculated using Eq. (4) if the 95% confidence interval of D_{cal} does not includes D_{true}. G_r and G_o were estimated using Eqs. (5) and (7), respectively, if the tests of the null hypotheses that β_1 and β_{c1} equal zero were rejected for $P < 0.01$.

Imaging Experiments With Gradient Scaling and Background Gradients

To evaluate the calibration protocol, experiments on the phantom were performed using 6 different simulated gradient scaling conditions both with and without background gradients. The 6 simulated gradient scaling conditions were null scaling $[c_x, c_y, c_z] = [1.0, 1.0, 1.0]$, gradient scaling along the x direction [1.05, 1.0, 1.0] and [1.1, 1.0, 1.0], gradient scaling along the combined y and z directions [1.0, 1.05, 1.10] and [1.0, 1.10, 1.05], and gradient scaling along the z direction [1.0, 1.0, 1.10]. The background gradient (G_o) was generated in the y direction using the linear gradient shims. The gradient scaling factors and background gradients were estimated for each condition. Estimated values were compared against the prescribed values.

Brain DTI experiments were also performed under the 6 gradient scaling conditions both with and without the introduced background gradients. Twelve diffusion-encoding directions were selected using a numerically optimized, minimum-energy–encoding scheme (Table 1).[18] The diffusion parameters: δ, Δ, and gradient amplitude of null scaling condition were 21 milliseconds, 32 milliseconds, and 3.5 G/cm, respectively, which generated a diffusion weighting of 966 s/mm^2. Two coronal 3-mm thick slices were obtained using cardiac gating (TR ~ 2 seconds). The other imaging parameters were TE of 74 milliseconds, field of view of 18 cm, and a 100 × 100 acquisition matrix size. Correction of eddy current distortion was initially performed using 2-dimensional registration algorithm in Flirt from the FSL software library.[20] The DTI data of all conditions were analyzed using both uncorrected and corrected gradients.

TABLE 1. Numerically Optimized, Minimum-Energy–Encoding Scheme[15]

Twelve Directions $[g_x, g_y, g_z]$
[−0.418, 0.824, 0.383], [0.502, 0.568, 0.652], [0.144, −0.430, −0.891], [0.698, 0.048, −0.714], [−0.090, −0.829, 0.552], [−0.224, −0.964, −0.142], [0.953, 0.194, 0.234], [0.617, −0.166, 0.769], [−0.918, 0.354, 0.180], [−0.577, 0.740, −0.344], [0.048, 0.276, −0.960], [−0.735, −0.617, 0.282]

Computer Simulation

Discrete tensor orientations over a range of azimuthal angles were simulated without noise to investigate the impact of gradient scaling errors and background gradients on DTI measures. A set of cylindrically symmetric DTs, with trace 2100 × 10^{-6} mm^2/s and a range of FA values between 0.0 and 0.9 were generated. The gradient errors were simulated by adding the background gradients 3% to 12% of G_{max} or scaling the gradients by discrete values between 1 and 1.2.

A numerical anisotropy phantom was generated with rectified Gaussian random noise[21] to demonstrate the effects of gradient errors on DTI measurements and evaluate the correction method. As shown in Figure 1A, the phantom is a circular disk with an MD of 700 × 10^{-6} mm^2/s. The FA was the distance of that voxel to the center of the disk normalized by the disk radius. Diffusion-tensors were assumed to be cylindrical symmetry, and each one was orientated along the vector pointing to that voxel from the center of the disk. In addition, a Monte Carlo simulation using a numerical isotropic phantom was used to investigate the minimum detectable gradient errors of the calibration protocol. Thirty repeated trials with SNR = 30 were used in the simulation. The ranges of studied gradient errors were between 1.012 and 1.050 for scaling factor and between 0.02 and 0.66 G/cm for background/residual gradient errors. The maximum diffusion-weighting gradient was set to be 4 G/cm.

RESULTS

Measurements in Diffusion Phantom

The calibration experiment with 6 simulated gradient scaling conditions was repeated 3 times within 1 month. Comparisons between the estimated gradient scaling factors, c, and the prescribed c are listed in Table 2. The estimated values were accurate to the third decimal. The overall uncertainty was less than 1% of the prescribed c. When a linear gradient shim was manually applied in the y direction, the calibration technique detected highly significant background gradients of 0.12 to 0.15 G/cm, which was 3.46% to 4.48% of the maximum diffusion gradient. When the linear and higher-order gradient shims were optimized on our system (eg, minimal B_o inhomogeneities), no significant residual gradients were detected.

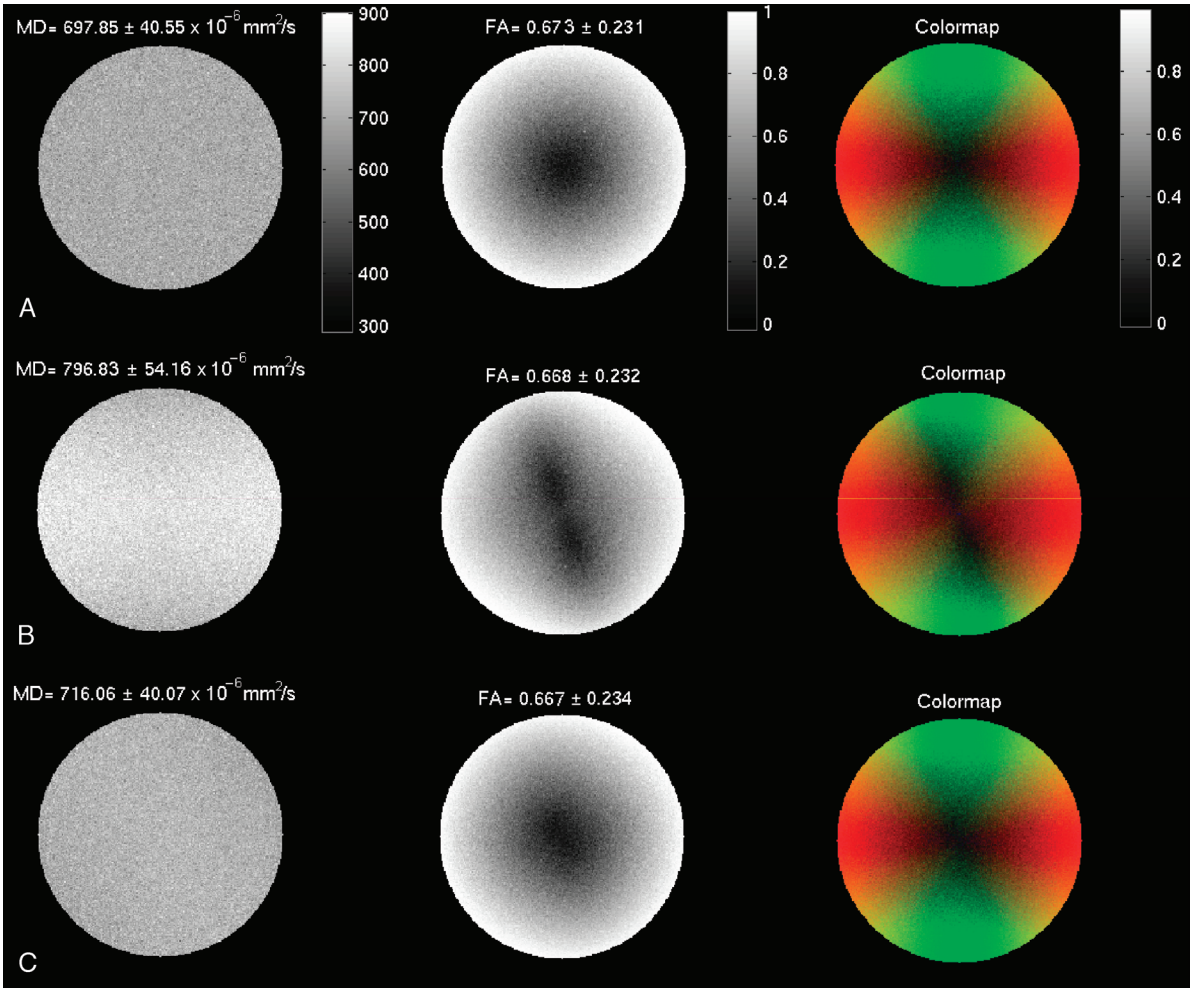

FIGURE 1. Diffusion tensor imaging measures of a numerical anisotropy phantom with and without gradient errors. A, Diffusion tensor imaging measures of a numerical anisotropy phantom with MD of 700 $\times$ 10^{-6} mm^2/s. The FA was increased with the distance from the center of the disk normalized by the disk radius. The DT of each voxel had the orientation along its position vector. The signal-to-noise ratio was 30. B, Diffusion tensor imaging measures under the influence of a combination of gradient errors (10% of the maximum DW gradient) including gradient scaling error along the *x* axis, background gradients along *y* axis, and residual gradients along *z* axis. C, Diffusion tensor imaging measures corrected by the total effective scaling vector.

The calibration protocol was also used to assess diffusion gradient performance on the 3.0T system for 13 months. No gradient errors were introduced. The results in Table 3 demonstrate that the gradient performance was very stable over this period. The gradient scaling was perfect for all sessions. Significant, but small, residual gradients were only detected on 2 occasions. Fairly systematic background gradients were observed in the *z* direction, although it is possible that this was caused by field distortions in the phantom. The results also demonstrated no significant changes

TABLE 2. Comparison of Prescribed *c* to the Estimated *c* for 6 Gradient Scaling Conditions

	Prescribed/Estimated		
Experiment	***x***	***y***	***z***
1	1/1.000 ± 0	1/1.0000 ± 0	1/1.0000 ± 0
2	1.05/1.052 ± 0.005	1/1.004 ± 0.006	1/1.001 ± 0.002
3	1.10/1.106 ± 0.002	1/1.004 ± 0.005	1/0.999 ± 0.002
4	1/1.000 ± 0	1.10/1.103 ± 0.011	1.05/1.057 ± 0.002
5	1/1.000 ± 0	1.05/1.056 ± 0.009	1.10/1.108 ± 0.004
6	1/1.004 ± 0.006	1.10/1.105 ± 0.008	1/1.004 ± 0.007

The uncertainty is one SD across repeated experiments. Each simulated condition was repeated for 3 dates and analyzed twice by drawing different ROIs.

TABLE 3. Results of Calibration Experiment Without Introduced Gradient Errors

Date (mm/dd/yr)	$c = [c_x, c_y, c_z]$	$G_r = [G_{rx}, G_{ry}, G_{rz}]$ (G/cm)	$G_o = [G_{ox}, G_{oy}, G_{oz}]$ (G/cm)
04/20/04	[1.000, 1.000, 1.000]	[0, 0, 0]	—
06/13/04	[1.000, 1.000, 1.000]	[0, −0.096, 0]	—
08/23/04	[1.000, 1.000, 1.000]	[0, 0, 0]	—
09/19/04	[1.000, 1.000, 1.000]	[−0.032, 0, 0]	[−0.053, −0, 0.048]
09/27/04	[1.000, 1.000, 1.000]	[0, 0, 0]	[−0.055, 0, 0.020]
02/17/05	[1.000, 1.000, 1.000]	[0, 0, 0]	[0, 0, 0.084]
03/02/05	[1.000, 1.000, 1.000]	[0, 0, 0]	[0, 0, 0.079]
04/26/05*	[1.000, 1.000, 1.000]	[0, 0, 0]	[0, 0, 0.022]
05/31/05*	[1.000, 1.000, 1.000]	[0, 0, 0]	[0, 0, 0]

At each date, the calibration experiment was repeated 5 times. c, G_r, and G_o were estimated using linear regression analyses [Eqs. (4), (5), and (7)] at significance levels of 95%, 99%, and 99%, respectively. The maximum gradient strength of our system is 3.98 G/cm.

*Our scanner system was upgraded during March 6 to April 15, 2005.

in diffusion gradient performance after a recent upgrade on the system.

Computer Simulation

The Monte Carlo simulation of minimum detectable gradient errors was showed in Figure 2. The estimation error (across 30 trials) of the gradient errors using the proposed calibration protocol increases dramatically when the gradient scaling factor was smaller than 1.015 (Fig. 2A) and background/residual gradients were smaller than 0.12 G/cm (Fig. 2B). These values were defined as the minimum detectable thresholds, and the calibration protocol yields reliable results when gradient errors are larger than the minimum detectable thresholds.

The computer-stimulated errors in MD and FA for gradient scaling factors, $c_x = 1.10$, are plotted in Figure 3A, C. The errors varied substantially both as functions of FA and the orientation of the tensor relative to the encoding directions. There was an increasing spread in the estimated MD as a function of tensor orientation for increasing FA. As the ideal tensors became more anisotropic, the estimated FA varied widely as a function of tensor orientation, but this spread decreased for highly anisotropic tensors. The computer-simulated errors in MD and FA with background gradients of 10% of the maximum diffusion gradient along the y axis are plotted in Figure 3B, D. Unlike the scaling factors (Fig. 3A), the background gradients demonstrated a minimum effect on the estimated MD (Fig. 3B). Significant errors (results not shown) in the estimated major eigenvector direction were observed for low anisotropy tensors, especially those that were highly oblique to the gradient error (either scaling error or background gradient) direction.

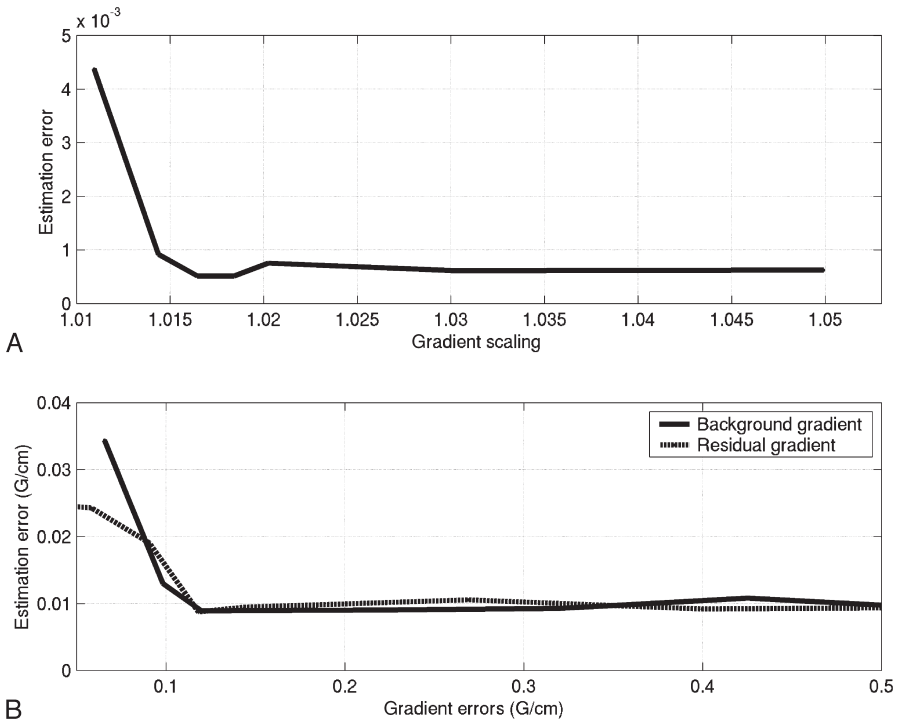

FIGURE 2. Computer simulation of minimum detectable gradient errors of the calibration protocol using an isotropy phantom. The signal-to-noise ratio was set to be 30. A, The simulated gradient scaling factor was increased from 1.012 to 1.050 (1.2%–5% error). B, The simulated background and residual gradient errors were increased from 0.02 to 0.66 G/cm (0.5%–17%, if G_{max} = 4 G/cm). The estimation error was defined as the SD of the estimated gradient errors across 30 repeated trials. The minimum detectable gradient thresholds were the minimum gradient errors that reach stable estimation error.

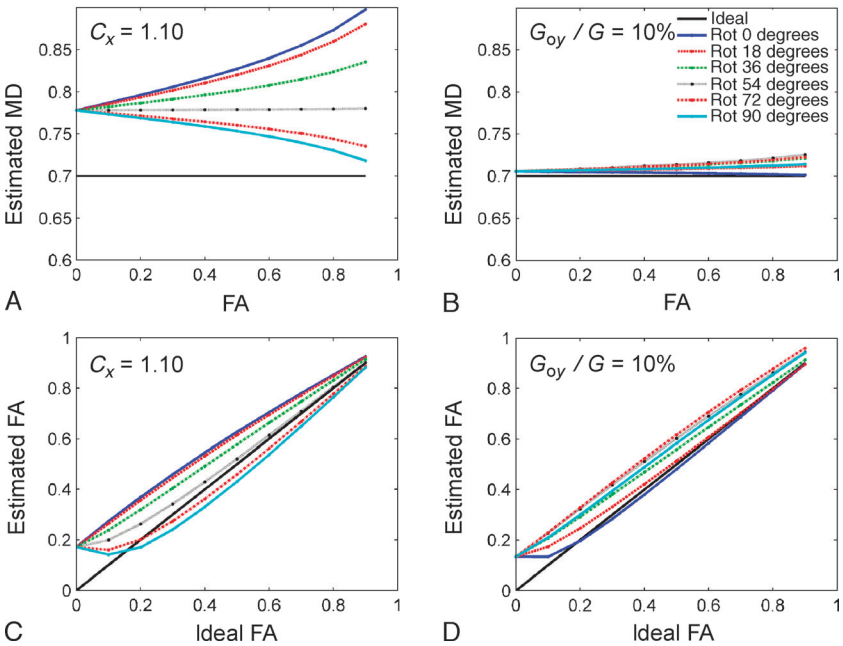

FIGURE 3. Estimated MD (A, B) and FA (C, D) for simulated noise-free DTs for a range of rotations with a gradient scaling factor $c_x = 1.10$ (A, C) and background gradients equal to 10% (B, D) of the maximum diffusion gradient along the *y* axis. The rotation angle is the angle between the major eigenvector of the DT and the *x* axis, and the units of MD are 10^{-3} mm^2/s.

The computer simulation of an anisotropy phantom showed that if diffusion-weighting gradients were underestimated, which happens when there were gradient scaling or residual gradients, the MD and FA were overestimated along the direction of scaling/residual gradient error (results not shown). For a 5% scaling error, the maximum overestimation was 3.99% ± 6.23% for MD, and FA errors ranged between −0.2 and 0.25 (larger at lower anisotropy, but near zero at high anisotropy). For a 5% background gradient error, MD was overestimated by 0.32% ± 5.78%, and FA errors ranged between −0.22 and 0.22 (results not shown).

The effects of combining gradient scaling error along *x* axis, background gradients along *y* axis, and residual gradients along *z* axis on DTI measurements were shown in Figure 1B. The overall MD was overestimated by 14%. The effects on FA and the color hue of the major eigenvector colormap were dependent on the tensor orientations. In Figure 1C, after retrospective correction using the total effective scaling vector [Eq. (9)], the overestimation of MD was minimized, and the patterns of the FA map and colormap were similar to the originals in Figure 1A.

Diffusion Measurements in Brain

The brain DTI experiment with 6 introduced gradient scaling conditions was repeated on 3 occasions with similar results. The MD, FA, and eigenvector colormaps from a pair of brain DTI experiments using null gradient scaling and a gradient scaling are shown in Figure 4. The maps in Figure 4A were acquired with null gradient scaling c = [1.0, 1.0, 1.0]. In Figure 4B, C, the gradient scaling condition was c =[1.1, 1.0, 1.0], with introduced background gradients. Before correction (Figure 4B), increased FA values were observed in most gray matter regions, and a red bias was apparent in the eigenvector colormap. After retrospective correction of the gradient scaling (Figure 4C), the apparent overestimation of FA and the color bias of the colormap were eliminated. Note that it is difficult to visualize the bias in MD based upon visualization of the map alone because of the maximum overestimation of MD is about 10% whose distribution depends on the orientation of DT and the noise variation is also about 10% in the brain MD image. The results were similar in other gradient scaling conditions (not shown), except the bias of eigenvector color was different according to the simulated conditions.

Histograms of whole-brain FA and the *x* component of the major eigenvector are plotted in Figure 5A and B, respectively. Some of the differences between histograms may be attributed to variations from image noise. However, there was an obvious shift in the histogram peaks when gradient scaling is present (red lines). The difference histogram peaks were shifted toward null-scaled condition after correction (blue lines).

DISCUSSION

The proposed calibration protocol may be performed regularly to monitor the systemic drifts in diffusion gradient and pulse sequence performances. The evaluation of gradient performances on our system demonstrated very minor gradient errors during a period of 13 months (Table 3). For the synthesized gradient error studies (Table 2), the protocol was capable of characterizing the scaling to within 0.7% or better. In addition, the minimum detectable gradient errors using this method were scaling errors of roughly 1.5% and background/residual gradients of roughly 3% (assuming G_{max} = 4 G/cm) (Fig. 2). A diffusion gradient error of this order would lead to errors in the estimated diffusion weighting of 1% or less. These results demonstrate that the protocol described here is a valid approach for quality control studies of gradient system performance.

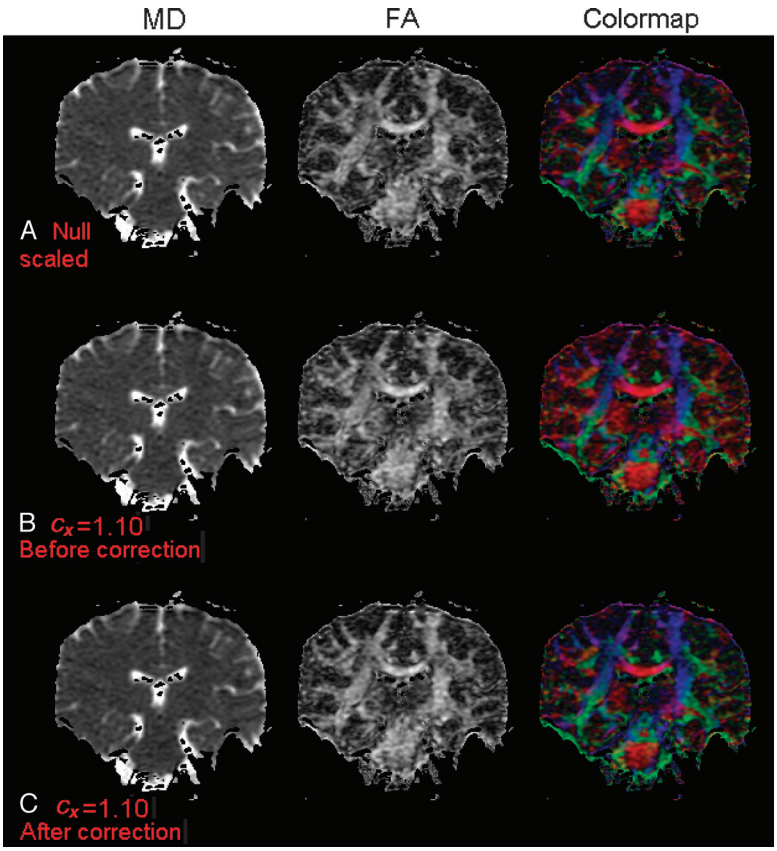

FIGURE 4. The MD, FA, and eigenvector colormaps from a pair of brain DTI experiments using both null gradient scaling ($c_{x,y,z}$ = 1.0) and gradient scaling (c_x = 1.1). The range of colorbar is 0 to 3000 × 10^{-6} mm^2/s for MD and 0 to 1 for FA and colormap. In the major eigenvector colormap, red, green, and blue denote the anatomical direction right-left, anterior-posterior, and superior-inferior, respectively. A, Maps with null gradient scaling. B, Maps with the gradient scaling demonstrate increased FA in gray matter regions, and the major eigenvector colormap has a red bias. C, Maps with the gradient scaling but corrected retrospectively.

An organic hydrocarbon fluid, *n*-undecane, was selected as the reference material for characterizing and calibrating the diffusion encoding gradients in this study. This material has isotropic diffusion properties with similar MD (1027 × 10^{-6} mm^2/s at 21°C) to that of brain tissue, relatively low flammability (flash point > 65°C), high chemical stability, and small diffusion temperature dependence (×1.9%/°C).[19] In addition, its chemical and diffusion properties will be stable for long periods, which may not be true for agar phantom, which can change water content over time. The most significant limitation with this material is the flammability, which, although low, does require specific storage requirements, which may be problematic in a clinical setting. The methodology described here would also be immediately applicable to other isotropic diffusing materials such as deionized water or glycerol. Indeed, we have compared measurements from both *n*-undecane and distilled water, which yielded the same results. One potential problem with water phantoms is that the temperature dependence is somewhat higher, so that absolute diffusion measurements may be less accurate. We have also observed more "vibrational" artifacts at the edges of water phantoms because of its lower viscosity.

Anisotropic phantoms have been suggested for diffusion calibration. Although they might be useful for specific applications such as testing tractography algorithms, this study and the study by Bammer et al[17] clearly demonstrate that an isotropic diffusion phantom is sufficient for characterizing scanner gradient performance. Anisotropic diffusion phantoms may also present certain challenges because the measurements will change with the phantom orientation.

Other researchers have also demonstrated that underestimation of gradients will lead to overestimation of diffusivities and tensor orientation errors.[5,8,13] The degree of error not only depends upon the gradient properties but also the tensor anisotropy and orientation relative to the encoding gradient directions. Thus, it would be very difficult to accurately correct the errors in computed scalar DTI maps such as MD or FA, and it is more preferable to correct the original diffusivities before tensor estimation. In this study, we have shown that the retrospective correction using a 6-element vector is effective. If the actual gradient waveforms are available, the method also provides the mathematical formula for prospective corrections.

Errors in the major eigenvector orientation will propagate into white matter tractography leading to errors in the estimated trajectories. The directional accuracy of diffusion weighting gradients is also extremely important in high-angular resolution diffusion imaging (HARDI). Although this study focused on DTI, the gradient calibration can easily be adapted to higher *b* value measurements obtained for HARDI,[22] q-ball imaging,[23] or diffusion spectrum imaging.[24] Similar to the case of DTI retrospective correction, the prescribed gradients of those diffusion imaging techniques may be corrected using the total effective scaling vector before subsequent reconstruction processes. To generalize this

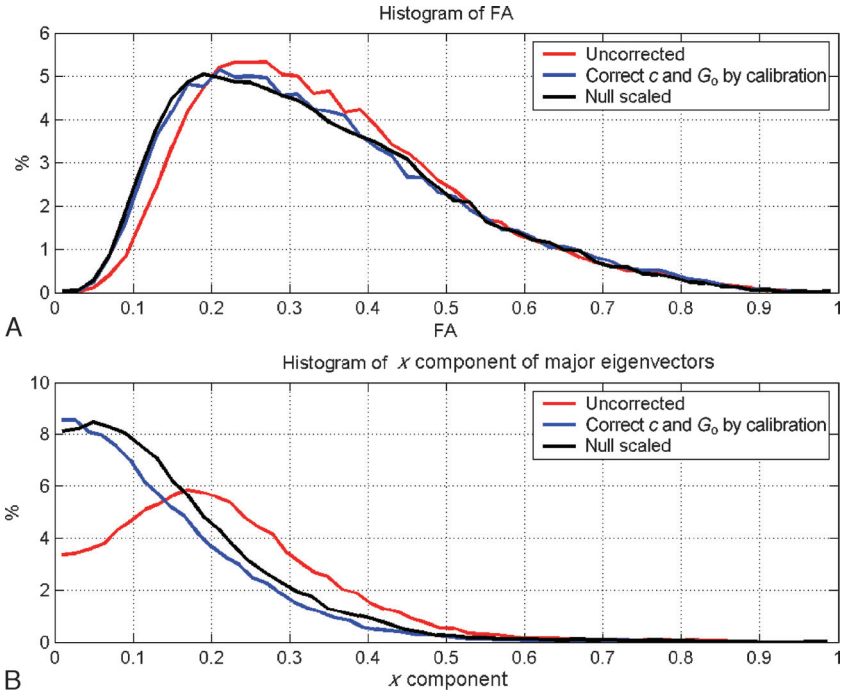

FIGURE 5. These plots were acquired from a pair of brain DTI experiments using null gradient scaling ($c_{x,y,z}$ = 1.0, black line) and gradient scaling (c_x = 1.1, red and blue lines). A, Whole-brain histograms of FA. B, Whole-brain histograms of x component of major eigenvectors.

technique for wide range of DW imaging applications, a phantom containing multiple fluids with a broad range of diffusivities may improve the utility.

Note that this method cannot distinguish background gradients from imaging gradients because they both have constant directions and amplitude. Therefore, Eq. (7) may combine effects of both background and imaging gradients. However, although inseparable, both gradient errors can be simultaneously corrected with opposite diffusion weighting gradients or by the total effective scaling vector [Eq. (9)] as long as the calibration protocol has the same imaging parameters as the DTI experiments. One limitation of this method is that it assumes that the residual gradients that arise from the diffusion-weighting gradients are along the same axis. Consequently, it will be suboptimal for calibrating the residual gradients arising from diffusion-weighting gradients of other axes.

In conclusion, a DTI calibration method using an isotropic phantom is described and evaluated. Diffusion tensor imaging images can be corrected retrospectively by correcting the diffusion encoding vectors used in the DT estimation. For a more comprehensive calibration protocol, this method may be combined with the method described by Bammer et al[17] to include the spatial calibration of gradient errors. Both the calibration and correction frameworks may be applied to general DW imaging including HARDI,[22] q-ball imaging,[23] and diffusion spectrum imaging.[24] In addition, these techniques may facilitate longitudinal study designs and the comparison of studies between scanners.

ACKNOWLEDGMENTS

The authors thank Jee Eun Lee for the support with the image registration. The authors also thank Paul Joseph Thottakara for help in phantom construction.

APPENDIX A

Figure A.1 illustrates a simplified example of the sources of gradient errors that may occur in the Stejskal-Tanner gradient pulse sequence for DW imaging experiments. These errors include gradient amplitude scaling errors (cG, where c is the scaling factor), constant background gradients (G_o), imaging gradients (G_i, G_{sl}), and residual gradients (G_r) from long-term eddy currents. Gradient errors contribute scaling, crossing, and quadratic terms in the diffusion signal attenuation.[3]

In the absence of background gradients and gradient scaling factors (Fig. A.1), the resultant gradient waveform is the combination of the pulsed diffusion gradients and the residual gradients. The analytical expression of the signal attenuation can be derived by integrations[3] of $\ln(S/S_o) = -D_{true}\int_0^{TE}\vec{k}(t)\cdot\vec{k}(t)\,dt$ and $\vec{k}(t') = \gamma\int_0^{t}\vec{G}(t')\,dt'$:

$$\ln(S/S_o) = D_{true}[BG^2 + R_1 G_r G + R_2 G_r^2] \qquad (A.1)$$

where G is the prescribed diffusion gradient and G_r is the residual gradient. The first term, BG^2, describes the signal attenuation caused by diffusion gradients where $B(\delta,\Delta) = -(\gamma\delta)^2(\Delta - \delta/3)$. The second term, $R_1 G_r G$, describes the attenuation from the coupling effect between diffusion and residual gradients, where

$$R_1(\delta,\Delta,t_2) = -\gamma^2\delta[\Delta(\Delta-\delta) - t_2^2] \qquad (A.2)$$

The last term, $R_2 G_r^2$, described the attenuation caused by residual gradients, where

$$R_2(\delta,\Delta,t_1,t_2,t_4) = -\gamma^2\left[\frac{1}{3}(\Delta-\delta)^3 + \frac{1}{3}t_4^3 + t_1 t_2^2 + 4t_2^2 t_4 - 2t_2 t_4^2 + \delta^2 t_4 + \delta(t_2^2 - t_4^2 + 4t_2 t_4)\right] \qquad (A.3)$$

δ and Δ are the diffusion gradient pulse duration and separation, respectively. The times t_1, t_2, t_3, and t_4 are the intervals between the

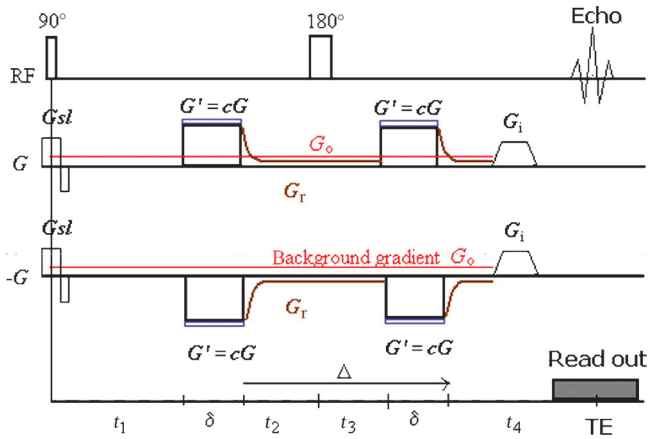

FIGURE A.1. Simplified waveforms of gradient errors (color lines) in a pulsed gradient spin-echo pulse sequence. G' (blue) denotes the scaled diffusion gradients: $G' = cG$, where c is the scaling factor. G_o (red), G_i (black), G_{sl} (black), and G_r (brown) denote the background, imaging, slice selection, and residual gradients, respectively. G and $-G$ symbolize opposite polarities of diffusion gradients in an arbitrary direction. In this study, both the background and the residual gradients are assumed to have constant amplitudes. δ and Δ are the diffusion gradient pulse duration and separation, respectively. t_1, t_2, t_3, and t_4 are the time intervals between the 90-degree radio frequency (RF) pulse and the onset of the first gradient, the end of the first gradient and the 180-degree RF pulse, the 180-degree RF pulse and the onset of the second gradient, and the end of the second gradient and the top of the echo, respectively. These time variables have effects on the coupling terms of diffusion gradients and gradient errors in the diffusion signal attenuation. In this study, $t_1 = t_4 = 3$ milliseconds, $t_2 = t_3 = 5.5$ milliseconds, and $\delta = 21$ milliseconds were used for both DW image calibration and brain DTI experiments.

90-degree RF pulse and the onset of the first gradient, the end of the first gradient and the 180-degree RF pulse, the 180-degree RF pulse and the onset of the second gradient, and the end of the second gradient and the top of the echo, respectively (Fig. A.1). Note that the residual gradient was assumed constant, and t_3 was set to be equal to t_2 in this derivation. Rewriting Eq. (A.1):

$$\ln(S/S_o) \approx D_{true} B c_{effR}^2 G^2. \tag{A.4}$$

The effective scaling factor for both the residual gradient and the gradient scaling factor is

$$c_{effR}^2 = c^2\left[1 + \frac{R_1 G_r}{BcG}\right] = c^2 + \frac{\beta_1}{BGD_{true}} \tag{A.5}$$

Note that the last term ($R_2 G_r^2$) in Eq. (A.1) has been omitted in Eq. (A.4) because this quadratic term of the residual gradient is usually negligible with respect to diffusion weighting gradient term (BG^2) and the cross-term ($R_1 G_r G$).

APPENDIX B

The model for the second linear regression analysis is

$$\ln(S_+/S_o) = \beta_{c2} G_c^2 + \beta_{c1} G_c + \beta_{co} + \varepsilon \tag{A.6}$$

where the β_c's and ε are the model coefficients and error, respectively, $\ln(S_+/S_o)$ is the signal attenuation of positive gradient polarity, and G_c is the corrected gradient strength. The signal attenuation with the present of background gradients (G_o) is

$$\ln(S_+/S_o) = D_{true}[BG_c^2 + O_1 G_o G_c + O_2 G_o^2] \tag{A.7}$$

where O_1 and O_2, derived by Stejskal and Tanner,[3] are functions of the following time intervals: δ, Δ, t_1, t_2, t_3, and t_4 (Fig. A.1). From Eqs. (A.6) and (A.7), the strength of the constant background gradient may be estimated as

$$G_o = \beta_{c1}/(D_{true} O_1) \tag{A.8}$$

Rearranging Eq. (A.7):

$$\ln(S_+/S_o) \approx D_{true} B c_{effO+}^2 G_c^2 \tag{A.9}$$

Note that the last term, $O_2 G_o^2$, in Eq. (A.7) has been omitted in Eq. (A.9). The effective scaling factor for the background gradient is

$$c_{effO\pm}^2 = 1 \pm \frac{O_1 G_o}{BG} = 1 \pm \frac{\beta_{c1}}{BGD_{true}}, \tag{A.10}$$

for positive (+) and negative (−) polarity.

REFERENCES

1. Le Bihan D. Molecular diffusion tissue microdynamics and microstructure. *NMR Biomed*. 1995;8(7–8):375–386.
2. Basser PJ, Pierpaoli C. Microstructural and physiological features of tissues elucidated by quantitative-diffusion-tensor MRI. *Magn Reson Med*. 1996;111:209–219.
3. Stejskal EO, Tanner JE. Spin diffusion measurements: spin echoes in the presence of time-dependent field gradient. *J Chem Phys*. 1965; 42:288–292.
4. Price WS, Kuchel PW. Effect of nonrectangular field gradient pulses in the Stejskal and Tanner (diffusion) pulse sequence. *J Magn Reson*. 1991;94:133–139.
5. Conturo TE, McKinstry RC, Aronovitz JA, et al. Diffusion MRI: precision, accuracy and flow effects. *NMR Biomed*. 1995;8:307–332.
6. Mori S, van Zijl PCM. Diffusion weighting by the trace of the diffusion tensor within a single scan. *Magn Reson Med*. 1995;33:41–52.
7. Jara H, Wehrli FW. Determination of background gradients with diffusion MR imaging. *J Magn Reson Imaging*. 1994;4:787–797.
8. LeBihan D, Basser PJ. Molecular diffusion and nuclear magnetic resonance. In: LeBihan D, ed. *Diffusion and Perfusion Magnetic Resonance Imaging*. New York: Raven Press, 1995:5–17.
9. Madi S, Hasan KM, Narayana PA. Diffusion tensor imaging of in vivo and excised rat spinal cord at 7 T with an icosahedral encoding scheme. *Magn Reson Med*. 2004;53:118–125.
10. Hunsche S, Moseley ME, Stoeter P, et al. Diffusion-tensor MR imaging at 1.5 and 3.0 T: initial observations. *Radiology*. 2001;221: 550–556.
11. Hasan KM, Arfanakis K, Alexander AL. A referenceless, balanced and efficient encoding scheme for diffusion tensor imaging. In: Proceedings of the 10th Annual Meeting of ISMRM; 2002; Honolulu, Hawaii.
12. Neeman M, Freyer JP, Sillerud LO. A simple method for obtaining cross-term–free images for diffusion anisotropy studies in NMR microimaging. *Magn Reson Med*. 1991;21(1):138–143.
13. Mattiello J, Basser PJ, LeBihan D. Analytical calculation of the b matrix in diffusion imaging. In: LeBihan D ed. *Diffusion and Perfusion Magnetic Resonance Imaging*. New York: Raven Press, 1995:77–90.
14. Nevo U, Hauben E, Yoles E, et al. Diffusion anisotropy MRI for quantitative assessment of recovery in injured rat spinal cord. *Magn Reson Med*. 2001;45(1):1–9.
15. Shimony JS, McKinstry RC, Akbudak E, et al. Quantitative diffusion-tensor anisotropy brain MR imaging: normative human data and anatomic analysis. *Radiology*. 1999;212(3):770–784.

16. Bodammer N, Kaufmann J, Kanowski M, et al. Eddy current correction in diffusion-weighted imaging using pairs of images acquired with opposite diffusion gradient polarity. *Magn Reson Med*. 2004;51(1):188–193.
17. Bammer R, Markl M, Barnett A, et al. Analysis and generalized correction of the effect of spatial gradient field distortions in diffusion-weighted imaging. *Magn Reson Med*. 2003;50:560–569.
18. Hasan KM, Parker DL, Alexander AL. Comparison of gradient encoding schemes for diffusion-tensor MRI. *J Magn Reson Imaging*. 2001;13:769–780.
19. Tofts PS, Lloyd D, Clark CA, et al. Test liquids for quantitative MRI measurements of self-diffusion coefficient in vivo. *Magn Reson Med*. 2000;43:368–374.
20. Jenkinson M, Smith SM. A global optimisation method for robust affine registration of brain images. *Med Image Anal*. 2001;5(2):143–156.
21. Pierpaoli C, Basser PJ. Toward a quantitative assessment of diffusion anisotropy. *Magn Reson Med*. 1996;36:893–906.
22. Frank LR. Characterization of anisotropy in high angular resolution diffusion-weighted MRI. *Magn Reson Med*. 2002;47: 1083–1099.
23. Tuch DS. Q-ball imaging. *Magn Reson Med*. 2004;52:1358–1372.
24. Wedeen VJ, Reese TG, Tuch DS, et al. Mapping fiber orientation spectra in cerebral white matter with Fourier-transform diffusion MRI. In: Proceedings of the 8th Annual Meeting of ISMRM; 2000; Denver, CO.

